Hybrid functionals applied to rare-earth oxides: The example of ceria

Juarez L. F. Da Silva,* M. Verónica Ganduglia-Pirovano, and Joachim Sauer
Institut für Chemie, Humboldt-Universität zu Berlin, Unter den Linden 6, D-10099 Berlin, Germany

Veronika Bayer
Institut für Physikalische Chemie, Universität Wien, Sensengasse 8/12, A-1090 Wien, Austria

Georg Kresse
Institut für Materialphysik, Universität Wien, Sensengasse 8/12, A-1090 Wien, Austria

(Received 21 July 2006; revised manuscript received 23 October 2006; published 22 January 2007; publisher error corrected 26 January 2007)

We report periodic density functional theory (DFT) calculations for CeO_2 and Ce_2O_3 using the Perdew-Burke-Ernzerhof (PBE0) and Heyd-Scuseria-Ernzerhof (HSE) hybrid functionals that include nonlocal Fock exchange. We study structural, electronic, and magnetic ground state properties. Hybrid functionals correctly predict Ce_2O_3 to be an insulator as opposed to the ferromagnetic metal predicted by the local spin density (LDA) and generalized gradient (GGA) approximations. The equilibrium volumes of both structures are in very good agreement with experiments, improving upon the description of the LDA and GGA. The calculated CeO_2 (O $2p$–Ce $5d$) and Ce_2O_3 (Ce $4f$-$5d4f$) band gaps are larger by up to 45% (PBE0) and 15% (HSE) than found in experiments. Furthermore, we calculate atomization energies, heats of formation, and the reduction energy of $2CeO_2 \rightarrow Ce_2O_3 + (1/2)O_2$. The latter is underestimated by $\sim 0.4-0.9$ eV with respect to available experimental data at room temperature. We compare our results with the more traditional DFT+U (LDA+U and PBE+U) approach and discuss the role played by the Hubbard U parameter.

DOI: 10.1103/PhysRevB.75.045121 PACS number(s): 71.15.Mb, 74.25.Bt, 71.23.An

I. INTRODUCTION

Cerium oxides (CeO_{2-x}, $0 < x < 1/2$) are interesting compounds with important applications in industrial catalysis, e.g., in automotive catalytic converters to decrease pollutants from combustion exhausts.[1] They are believed to be key materials in the future hydrogen production technology,[2,3] in particular for the water-gas-shift reaction and the conversion of ethanol and ethanol-water mixtures into dihydrogen. The beneficial role of cerium oxides in catalysis has been mainly attributed to their oxygen storage capacity, i.e., their ability to easily take up and release oxygen under oxidizing and reducing conditions, respectively.[1,4,5] Thus, having a theoretical approach that is able to describe the changes in the oxidation state of the multivalent cerium atoms appears desirable. In terms of the electronic structure, partially reduced ceria represents an intermediate case between CeO_2 and Ce_2O_3, on which the present work focuses.

The quantitive prediction of the chemical and physical properties of systems containing multivalent metals, in particular lanthanide species, requires an accurate description of the f states and has been a challenge to density functional theory (DFT) calculations. The local density (LDA) and generalized gradient (GGA) approximations to the exchange-correlation (XC) energy functional often yield a qualitatively *incorrect* behavior for the case in which the f-orbital overlaps are small, the bands narrow, and the electrons nearly localize.[6] In Ce_2O_3, the cerium atoms are in a trivalent configuration ($4f^1$), the $4f$ orbital localizes, and the material behaves like a typical antiferromagnetic (AF) Mott-Hubbard insulator.[7,8] The dioxide, on the other hand, is an insulator and the Ce atoms are tetravalent ($4f^0$).[9] Existing first-principles calculations[10–13] have been only partly successful in providing a unified description of the ground state properties of both cerium oxides.

Two different approximations for modeling the Ce_2O_3 and CeO_2 oxides are often adopted in DFT. The Ce $4f$ states are treated either as part of the core or explicitly as valence states. The former approach describes Ce_2O_3 as an insulator by construction, but it is not applicable to CeO_2. The approach that treats the Ce $4f$ states as valence states resulted in the expected insulating ground state for CeO_2, but a ferromagnetic (FM) metallic ground state for Ce_2O_3. A likely reason for this failure is the incomplete cancellation of the Coulomb self-interaction in the density functionals used, which stabilizes delocalized solutions. As a result, the electronic structure of magnetic materials with strongly localized electrons is generally not correctly reproduced.[14,15]

Pragmatic approaches that have been developed to overcome the limitations of the LDA and GGA functionals, such as the self-interaction correction[16] and the DFT+U approach,[6] have been recently applied to cerium oxides.[11,17] But subtle details of the actual implementation can strongly influence the results. For DFT+U, the band gaps and the energetics depend on the Hubbard U parameter, the choice of the localized orbitals, and the underlying exchange-correlation functional (LDA or GGA).

A different possibility to reduce the improper self-interaction is the use of hybrid functionals in which a fixed amount of nonlocal Fock exchange is added to local (LDA) or semilocal (GGA) XC functionals. Despite the important impact of hybrid functionals in molecular quantum chemistry, B3LYP in particular,[18] their applications to periodic solids used to be linked to Gaussian basis sets.[15,19–24] The reason is the large computational effort to evaluate the nonlocal Fock exchange in extended periodic systems using a plane-wave basis set. Due to the progress in plane-wave-based

algorithms[25,26] and computer speed, hybrid functionals such as the Heyd-Scuseria-Ernzerhof[27,28] (HSE) and the Perdew-Burke Ernzerhof[29–31] (PBE0) functionals have been recently implemented in widely used plane-wave basis set codes.[32–34]

In this work, we report a hybrid functional study of bulk CeO_2 and Ce_2O_3 using the PBE0 and HSE hybrid functionals within the framework of the plane-wave projector augmented wave (PAW) formalism,[35–37] and compare with the LDA, the Perdew, Burke, and Ernzerhof GGA (from now on referred to as PBE), LDA+U, and PBE+U descriptions of these systems. We calculate the ground state structural, electronic, and magnetic properties as well as atomization energies and heats of formation. We also present results for the reduction energy of $2CeO_2 \rightarrow Ce_2O_3 + \frac{1}{2}O_2$. Selected PBE calculations were performed using the full-potential (linearized) augmented plane-wave plus local orbitals (FPL/APW+LO) method.[38]

II. THEORETICAL APPROACH AND COMPUTATIONAL DETAILS

Spin-polarized calculations were performed using different XC energy functionals. The hybrid PBE0 (Refs. 29–31) and HSE (Refs. 27 and 28) functionals were used. In both cases 75% of the well-known PBE exchange[39] is combined with 25% of the nonlocal Fock exchange, and the correlation functional corresponds to that in the PBE functional. The HSE and PBE0 functionals differ in the treatment of the long-range part of the Fock exchange interaction with the former being computationally advantageous. The HSE functional cuts off the long-range tail of the Coloumb $1/r$ kernel using the complementary error function, allowing for a coarse k-point sampling of the nonlocal exchange kernel.[33] Since this cutoff also slightly reduces the (formally) 25% Fock exchange experienced by the electrons, the HSE and PBE0 functionals give similar, but not identical, descriptions for solid state systems. Generally band gaps tend to be slightly smaller using the HSE functional, whereas the energetics are very similar for both functionals.[33] We note that the use of 25% nonlocal Fock exchange has been justified using the adiabatic-connection fluctuation dissipation theorem,[29] and there is ample evidence that this value gives accurate results for a large class of materials, including metals.[28,33] In the present case, the parameter ω in the HSE functional was set to 0.3 Å=0.158 a.u. for both the local density part as well as the nonlocal Fock part. These are the parameters originally suggested for the HSE03 functional, but differ from those actually applied in Refs. 27 and 28 [see also Ref. 40].

The LDA (Ref. 41) and PBE (Ref. 39) functionals were also employed. Furthermore, a Hubbard U term was added to the plain LDA and PBE functionals[6] (LDA+U and PBE+U) employing the rotationally invariant approach proposed by Dudarev *et al.*,[42] in which only the difference ($U_{\text{eff}}=U-J$) between the Coulomb U and exchange J parameters enters. Values of $U_{\text{eff}}=5.30$ and 4.50 eV were used in the LDA+U and PBE+U calculations, respectively, which were calculated self-consistently by Fabris *et al.*[13] using the linear-response approach of Cococcioni and de Gironcoli.[43]

The Kohn-Sham equations were solved using the projector augmented wave method,[35–37] as implemented in the Vienna *ab initio* simulation package (VASP).[44,45] The calculations use a yet unreleased version, which includes the nonspherical one-center contributions to the PBE potential and hybrid functionals. For comparison, selected PBE calculations were made using another full-potential approach, namely, the full-potential L/APW+LO method[38] as implemented in the WIEN2k program,[46,47] which is a combination of the linearized augmented plane-wave method[48] and the augmented plane-wave plus local orbitals method.[49]

In the PAW method, the interaction between the ions and electrons is described by the standard frozen-core potentials provided within the VASP package, which were generated according to the procedure outlined in Ref. 36. We treated the Ce $(4f,5s,5p,5d,6s)$ and O $(2s,2p)$ electrons as valence states, while the remaining electrons were kept frozen as core states. A plane-wave cutoff energy of 400 eV was used. The augmentation charges were evaluated using an additional grid, which contained eight times more points than the grid for the wave functions determined from the cutoff energy. The projection operators were evaluated in reciprocal space.

In the mixed L/APW+LO method, the L/APW+LO wave functions inside the atomic spheres with radius of 1.16 and 0.74 Å for Ce and O atoms, respectively, are composed by a combination of APW+LO basis functions ($l=0,1,2,3$ for Ce and $l=0,1$ for O) and LAPW basis functions for all higher angular momenta up to 12. Furthermore, local orbitals were set to specifically treat the Ce $5s$, $5p$, and $5d$ orbitals, as well as the O $2s$ orbital. The L/APW+LO wave functions in the interstitial region were represented using plane waves with kinetic energy up to 250 eV, whereas for the potential representation in the interstitial region, plane waves with kinetic energy up to 3500 eV were considered. Inside of the atomic spheres, the representation of the potential considered terms with angular momentum up to 6. Furthermore, nonspherical matrix Hamiltonian elements are considered up to $l=6$.

The Brillouin-zone integrations were performed using Monkhorst-Pack grids.[50] The hybrid calculations were carried out using a $(6\times6\times6)$ mesh for both systems, whereas for the remaining calculations, $(10\times10\times10)$ and $(10\times10\times5)$ meshes were employed for CeO_2 and Ce_2O_3, respectively. We note that the hybrid functional calculations are converging rapidly with the k-point grid, since both systems become wide band gap insulators. Thus results using a $(6\times6\times6)$ mesh are virtually identical to those obtained using a $(4\times4\times4)$ grid.

III. RESULTS

A. Equilibrium volumes

Bulk CeO_2 and Ce_2O_3 have fluorite-type (face-centered cubic, $Fm\bar{3}m$) and sesquioxide A-type (hexagonal, $P\bar{3}m1$) structures, respectively, with one formula unit per primitive unit cell (see Fig. 1). In CeO_2, the Ce and O atoms are eight- and four-fold coordinated, respectively, with an experimental Ce-O bond length of 2.34 Å.[51–54] In Ce_2O_3 the Ce atoms are seven-fold coordinated with experimental Ce-O bond lengths of 3×2.34, 1×2.43, and 3×2.69 Å,[8,55] while two of the O atoms are four-fold coordinated and the third O atom is six-

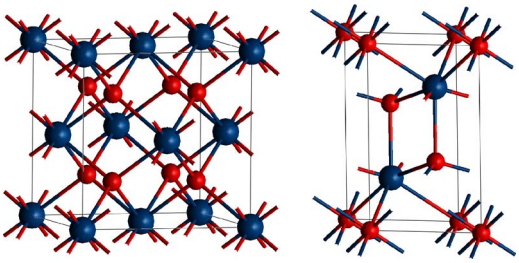

FIG. 1. (Color online) Fluorite-type structure (face-centered cubic, $Fm\bar{3}m$) of CeO_2 (left) and the sesquioxide A-type structure (hexagonal, $P\bar{3}m1$) of Ce_2O_3 (right), respectively. Large blue and small red balls indicate Ce and O atoms, respectively.

fold coordinated. All atomic positions in the fluorite-type structure are fully constrained by the space group symmetry, while in the hexagonal structure there are two free internal parameters (u_{Ce}, u_O) in addition to the two lattice constants (a_0, c_0).

The LDA, PBE, LDA+U, PBE+U, PBE0, and HSE equilibrium volumes V_0 were calculated by minimizing the stress tensor and all internal degrees of freedom. To avoid problems resulting from the basis set change upon changing the volume (Pulay stress), the cutoff energy was increased to 800 eV (LDA, PBE, LDA+U, and PBE+U) or a uniform correction to the stress tensor was applied (PBE0 and HSE). The bulk moduli B_0 were obtained by fitting the calculated total ground state energies for selected relaxed structures with fixed volumes to Murnaghan's equation of state.[56] The high computational cost of the hybrid computations precluded energy minimization at various volumes; hence no bulk moduli are reported for the hybrid functionals. In Tables I and II our calculated bulk properties are compared to available experimental data.

The hybrid PBE0 and HSE functionals yield the same equilibrium volume $(V_0 = a_0^3/4)$ for CeO_2, which is underestimated by only 1.1% compared to the experimental volume.[51,52,54] For Ce_2O_3, the equilibrium volume $(V_0 = \sqrt{3}a_0^2 c_0/2)$ of the AF spin configuration is also underestimated by about 1% in the PBE0 and HSE calculations compared to the experimental volume.[55] The general agreement between the lattice constants of both oxides and experiment is very satisfactory. Our hybrid functional results are in line with the tendency of hybrid functional calculations to underestimate equilibrium volumes recently observed for selected metallic, semiconducting, and simple oxide systems.[28,33]

TABLE I. Bulk properties of CeO_2 in the fluorite-type structure. Equilibrium lattice constant a_0, bulk modulus B_0, and atomization energy E_{at}, per formula unit.

Method	XC	a_0 (Å)	B_0 (Mbar)	E_{at} (eV)
PAW[a]	PBE0	5.39		19.13
PAW[a]	HSE	5.40		19.70
PAW[a]	LDA	5.37	2.01	24.55
PAW[a]	PBE	5.47	1.72	21.04
L/APW+LO[a]	PBE	5.47	1.70	21.15
PAW[a]	LDA+U	5.40	2.10	
PAW[a]	PBE+U	5.49	1.80	
Expt.		5.406[b]	2.30[b]	
Expt.		5.411[c,e]	2.04,[d] 2.20[e]	

[a]Present work.
[b]Reference 51.
[c]Reference 52.
[d]Reference 53.
[e]Reference 54.

The LDA and PBE results for CeO_2 reflect the expected underestimation (by 2.2%) and overestimation (by 3.3%) of the equilibrium volume, respectively, which are characteristics of these functionals (see, e.g., Refs. 57 and 58). The agreement between the PAW and the FP-L/APW+LO calculations is excellent, both for the lattice constants, as well as for the bulk moduli, and the comparison to experiment is fairly decent. The combination of overestimated equilibrium volumes and underestimated bulk moduli, typical of PBE, can be seen as well in Table I.

Yet, in contrast to CeO_2, the equilibrium volumes obtained for Ce_2O_3 using the LDA and PBE are far from being satisfactory. Both LDA and PBE underestimate V_0 by 8.9% and 2.7%, respectively. We note that our LDA and PBE results for both the equilibrium lattice constants and the bulk modulus are in good agreement with most of the previous first-principles calculations.[10,11,13,59,60]

Thus, the PBE0 and HSE results are in much better agreement with experiment than the LDA and PBE ones. The improvement of the hybrid calculations over local and semilocal functionals goes beyond the lattice constants as discussed in the next section. The improvement is particularly noticeable for the Ce_2O_3 case. For the hybrid functionals, the equilibrium volume usually lies in between the LDA and GGA values, but for Ce_2O_3 the volume increases from the GGA to HSE and PBE0 results. As shown below, a single electron localizes in a Ce 4f state per Ce atom for the hybrid functionals, effectively removing any hybridization with the conduction and valence bands. In the local and semilocal functionals, the Ce 4f states below the Fermi level are delocalized and show spurious bonding interactions with the oxygen 2p states leading to a much too small equilibrium volume. This is a first hint that the description of the bonding properties is much improved using the hybrid functionals.

For the DFT+U case, the calculated CeO_2 and Ce_2O_3 equilibrium volumes depend significantly on the description of the standard DFT part (LDA versus PBE). The LDA+U scheme underestimates V_0 by 0.6% and 3.2% for CeO_2 and Ce_2O_3, respectively, whereas, the corresponding PBE+U volumes deviate by +4.5% and +3.6%. Hence the inclusion of U in either LDA or PBE changes the volume only little for CeO_2 (by up to +2%), but strongly increases the volume of Ce_2O_3 (+6%). This is similar to the hybrid functionals and suggests that the LDA+U approach gives a reasonable account of the electron localization. It is noteworthy that the LDA+U values appear to be closer to experiment and the hybrid approaches than the PBE+U results. A recent publication of Fabris *et al.*[61] also indicated a better performance of LDA+U than PBE+U for the description of reduced ceria surfaces.

As usual, the volume V_0 depends on the parameter U_{eff}, as shown in Fig. 2. The results were obtained by minimizing the

TABLE II. Bulk properties of Ce_2O_3 in the sesquioxide A-type structure. Equilibrium lattice constants (a_0, c_0), internal parameters (u_{Ce}, u_O), bulk modulus B_0, the total magnetic moment per unit cell (per cerium atom in parentheses), and atomization energy E_{at}, per formula unit. FM and AF indicate ferromagnetic and antiferromagnetic spin configurations, respectively.

Method	XC	Spin	a_0 (Å)	c_0 (Å)	u_{Ce}	u_O	B_0 (Mbar)	m (μ_B)	E_{at} (eV)
PAW[a]	PBE0	FM	3.87	6.06	0.2460	0.6459		2.00 (1.00)	32.44
PAW[a]	PBE0	AF	3.87	6.07	0.2459	0.6455		0.00 (0.99)	32.45
PAW[a]	HSE	FM	3.87	6.07	0.2459	0.6459		2.00 (1.00)	33.54
PAW[a]	HSE	AF	3.87	6.08	0.2459	0.6454		0.00 (0.99)	33.55
PAW[a]	LDA	FM	3.77	5.88	0.2429	0.6413	1.38	2.00 (0.87)	40.41
PAW[a]	LDA	AF	3.73	5.93	0.2430	0.6354	1.38	0.00 (0.15)	40.35
PAW[a]	PBE	FM	3.83	6.08	0.2459	0.6430	1.14	2.00 (0.89)	34.80
PAW[a]	PBE	AF	3.85	6.10	0.2484	0.6419	1.01	0.00 (0.76)	34.72
L/APW+LO[a]	PBE	FM	3.85	6.04	0.2459	0.6435	1.13	2.00 (0.85)	34.60
PAW[a]	LDA+U	FM	3.87	5.93	0.2441	0.6463		2.00 (0.97)	
PAW[a]	LDA+U	AF	3.86	5.96	0.2446	0.6456	1.30	0.00 (0.97)	
PAW[a]	PBE+U	FM	3.92	6.18	0.2471	0.6448		2.00 (0.97)	
PAW[a]	PBE+U	AF	3.92	6.18	0.2473	0.6447	1.11	0.00 (0.97)	
Expt.[b]			3.89	6.06	0.245	0.647			
Expt.					0.251[c]	0.648[d]		2.17[d]	

[a]Present work.
[b]Reference 55.
[c]Reference 8; results obtained at a temperature of 4.2 K.
[d]Reference 8.

stress tensor. Both the LDA+U and PBE+U lattice constants increase almost linearly with U_{eff} for both cerium oxides. The slope of the curve is significantly steeper for Ce_2O_3 (note the different scale). Only the LDA+U curves approach or intersect the experimental line at a value of roughly U_{eff} =8.0 eV. This value is, however, larger than the effective U_{eff} determined by perturbation theory (5.30 eV),[13] and its use would worsen other materials properties, in particular, formation energies (see below).

B. Electronic structure

Although optical properties and band gaps are not ground state properties, it has become a common practice to compare DFT one-electron energies with experimentally measured quasiparticle spectra. In Fig. 3, we present results for the CeO_2 and Ce_2O_3 spin-projected total and local density of states (DOS). In CeO_2, all valence Ce states, including the 4f states, are empty and the system is a wide gap insulator with a measured fundamental band gap[62] (E_g) of 6.0 eV between the valence and conduction bands, which are formed predominantly by O 2p and Ce 5d states, respectively. The vacant 4f states lie in the gap. In Ce_2O_3, on the other hand, one electron per Ce atom populates a Ce 4f state, resulting in a single occupied Ce 4f peak, which lies in the E_g gap, 2.4 eV ($E_{g\text{-}f}$) below the conduction band,[7] which is formed to a large extent by Ce 5d+4f states. As $E_{g\text{-}f}$, we denote the energy difference between the lowest 4f state and the vacant conduction band. This 4f state is empty (lowest unoccupied) for CeO_2 and occupied by a single electron for Ce_2O_3.

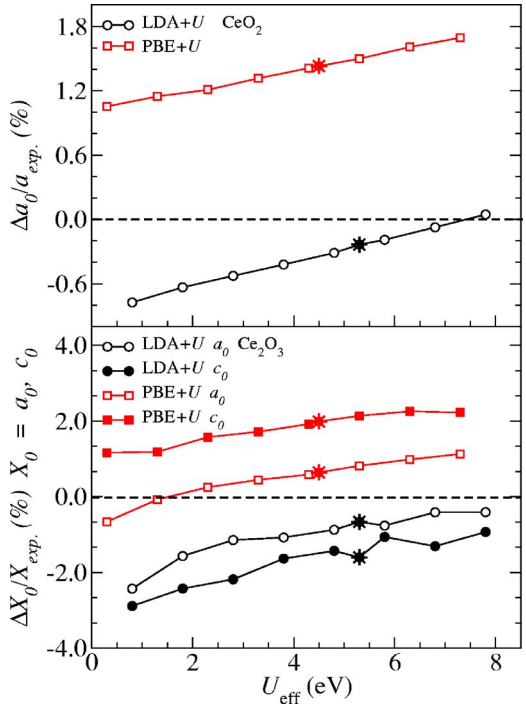

FIG. 2. (Color online) Equilibrium lattice constants of CeO_2 and Ce_2O_3 as a function of U_{eff}. The lattice constants are given in percentages with respect to the experimental values (a_0=5.41 Å for CeO_2; a_0=3.89 Å, c_0=6.06 Å for Ce_2O_3). The stars indicated the results obtained with the calculated U_{eff} using the linear-response approach of Ref. 43.

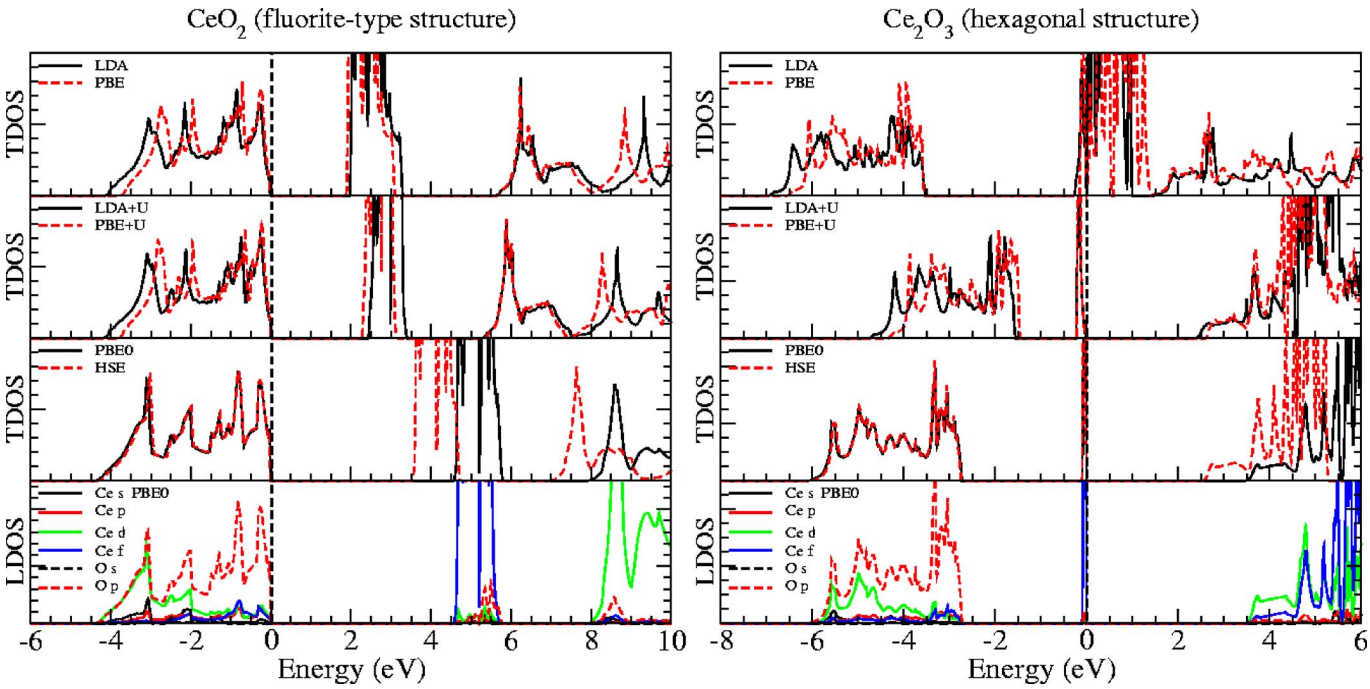

FIG. 3. (Color online) Total and local density of states (TDOS and LDOS) calculated with different XC energy functionals. Zero in the energy x axis indicates the top of the occupied valence band. All DOSs are calculated at the optimized geometries. For Ce_2O_3, only the spin-up component of the AF spin solution is shown.

For CeO_2, the local, semilocal, and hybrid functionals yield an insulating solution, which is in agreement with spectroscopic and optical reflectivity measurements.[9,62,63] The empty Ce 4f states can be identified in the band gap (see Fig. 3). A slight admixture of Ce d and Ce f character into the predominantly O 2p valence band can be observed (see also Ref. 9). As usual, LDA and PBE results show the typical underestimation of band gaps, namely, 5.61 (LDA) and 5.64 eV (PBE). These values correspond to the energy difference between the highest occupied and the lowest unoccupied band located above the Ce 4f states in the gap.

The hybrid functionals instead, overestimate the band gap, specifically, 7.93 (PBE0) and 6.96 eV (HSE). The ~1 eV larger value for the PBE0 case is in line with previous studies[33] and related to the use of a screened exchange interaction in the HSE functional as opposed to the bare Coloumb kernel in the PBE0 case.

For the magnetic Ce_2O_3 system, PBE0 and HSE yield an AF insulating ground state driven by the ordering of the partially occupied Ce 4f orbitals in the band gap. This ordering is consistent with magnetic susceptibility measurements.[8] The AF solution is by 6 (PBE0) and 5 meV (HSE) lower in energy than the FM insulating solution. By inspecting the local DOS, we found an occupation of the Ce 4f states by almost one electron, which gives rise to a magnetic moment of $\approx 1.0\mu_B$ per Ce atom, in good agreement with the experimental value of $1.085\mu_B$.[8] The calculated magnetic moments are given in Table II. We also found that, similarly to CeO_2, the PBE0 functional overestimates the $Ce_2O_3 E_{g\text{-}f}$ band gap, wheres the HSE results are in excellent agreement with experiment [3.5 (PBE0) and 2.5 eV (HSE) with the experimental value being 2.4 eV].

The DOS in Fig. 3 indicates that local and semilocal functionals yield a metallic solution for the ground state of Ce_2O_3; however, a careful analysis of the band structure shows a semi-metallic character with a mini-band-gap of ~10 meV ($E_{g\text{-}f}$) in the PBE case. The FM solution has a magnetic moment of $2.0\mu_B$ per formula unit, which is 60 (LDA) and 110 meV (PBE) lower in energy than the AF solution. We note that the mini-band-gap vanishes in the LDA using reliable all-electron methods (PAW and FP-L/APW+LO), as reported recently by Kresse *et al.*[12] Fabris *et al.* incorrectly calculated a large $E_{g\text{-}f}$ gap for Ce_2O_3 even using the LDA functional but this result was an artifact of an inaccurate pseudopotential.[12,13]

The pragmatic DFT+U approach works again reasonably well for Ce_2O_3 and gives results similar to the hybrid functional. An AF insulating ground state is obtained with the AF solution being 3 (LDA+U) and 2 meV (PBE+U) lower in energy than the FM configuration. We found that the precise structure and volume play a significant role in the magnitude by which the AF solution is preferred. For instance, using the experimental Ce_2O_3 structure, the AF-FM energy difference increases by one order of magnitude to about 50 meV.

A major difference between the hybrid functional and DFT+U approach arises for the size of the E_g and $E_{g\text{-}f}$ band gaps (see Fig. 3). Specifically, the CeO_2 band gap (E_g =5.3 eV in DFT+U) is smaller than the experimental one (6.0 eV) and much smaller than the PBE0 and HSE values (7.9 and 7.0 eV). In the case of Ce_2O_3, the deviations are less severe. In particular, the DFT+U $E_{g\text{-}f}$ gap equals 2.4 (LDA+U) and 2.6 eV (PBE+U), while the experimental value and HSE values are 2.4 and 2.5 eV, respectively. One could argue that in order to improve the agreement with experiment different values of U_{eff} should be used. However, from the calculated band gaps at the Γ point (see Fig. 4) as a function of U_{eff}, we conclude that the fundamental gap E_g in CeO_2 is

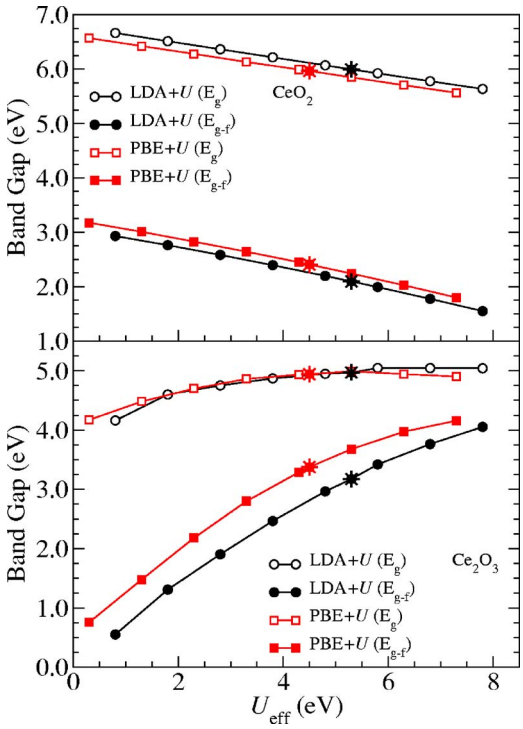

FIG. 4. (Color online) CeO_2 and Ce_2O_3 band gap E_g and position of the Ce $4f$ states (see text) $E_{g\text{-}f}$ at the Γ point, calculated as a function of U_{eff}. Results are obtained for the theoretical equilibrium volumes. The stars indicate the results obtained with the calculated U_{eff}.

roughly constant. This is not particularly astonishing, since the U_{eff} acts on the Ce $4f$ states only, and the valence and conduction bands have predominantly O $2p$ and Ce $5d$ character. The position of the $4f$ states (cf. Fig. 4), reported as $E_{g\text{-}f}$—the difference between the eigenvalue of the lowest $4f$ state and the lowest unoccupied band at the Γ point—is strongly affected by U_{eff} in Ce_2O_3. For Ce_2O_3, an increase of U_{eff} shifts the occupied Ce $4f$ state away from the conduction band, as expected. In CeO_2 an increasing U_{eff} shifts the empty f states toward the conduction band, in turn reducing the values of $E_{g\text{-}f}$.

C. Thermodynamic properties

At zero temperature, the heats of formation ΔH_f of bulk CeO_2 and Ce_2O_3 are defined by

$$\Delta H_f^{CeO_2} = E_{tot}^{CeO_2} - E_{tot}^{\text{bulk Ce}} - E_{tot}^{O_2}, \quad (1)$$

$$\Delta H_f^{Ce_2O_3} = E_{tot}^{Ce_2O_3} - 2E_{tot}^{\text{bulk Ce}} - (3/2)E_{tot}^{O_2}, \quad (2)$$

and the reduction energy of CeO_2 to Ce_2O_3 $\left(2CeO_2 \rightarrow Ce_2O_3 + \frac{1}{2}O_2\right)$ is given by

$$\Delta H^{CeO_2 \rightarrow Ce_2O_3} = E_{tot}^{Ce_2O_3} + (1/2)E_{tot}^{O_2} - 2E_{tot}^{CeO_2}. \quad (3)$$

TABLE III. Lattice constant of Ce metal in the face-centered cubic structure and O_2 molecule bond length, and atomization energies per Ce atom and per O_2 molecule.

Method	XC	α-Ce metal a_0 (Å)	α-Ce metal E_{at} (eV)	O_2 d_0 (Å)	O_2 E_{at} (eV)
PAW[a]	PBE0	4.67	2.61	1.19	5.37
PAW[a]	HSE	4.66	3.29	1.19	5.41
PAW[a]	LDA	4.51	5.51	1.22	7.55
PAW[a]	PBE	4.73	4.58	1.22	6.22
L/APW+LO[a]	PBE	4.72	4.41	1.22	6.21
Expt.		4.83[b]	4.32[c]	1.21[d]	5.25[d]

[a]Present work.
[b]Reference 64; α-Ce (a_0=5.16 Å for γ-Ce).
[c]Reference 67.
[d]Reference 68.

$E_{tot}^{CeO_2/Ce_2O_3/\text{bulk Ce}/O_2}$ indicates the total energies of CeO_2, Ce_2O_3, bulk Ce, and O_2 per formula unit, respectively. Furthermore, we calculate also the atomization energies E_{at}. For CeO_2, $E_{at}=E_{tot}^{Ce}+2E_{tot}^{O}-E_{tot}^{CeO_2}$, where $E_{tot}^{Ce/O}$ indicates the total energies of the free Ce and O atoms, respectively. Thus, Eqs. (1)–(3) can be rewritten using the atomization energies, in which $E_{tot}^{CeO_2/Ce_2O_3/\text{bulk Ce}/O_2}$ should be replaced by $-E_{at}^{CeO_2/Ce_2O_3/\text{bulk Ce}/O_2}$.

Metallic nonmagnetic α-Ce has been considered in the face-centered cubic structure,[64] while the spin-polarized calculation for the O_2 molecule was performed in an orthorhombic box [$(12\times13\times14)$ Å^3]. For the calculation of the atomization energies we evaluated the spin-polarized total energy of the free O and Ce atoms using the same orthorhombic box. For both the Ce and O atoms, no constraint was imposed on the one-electron occupation. For the particular case of O_2 a hard oxygen PAW potential with a cutoff energy of 1000 eV was employed. The atomization energies are reported in Tables I, II, and IV. Zero-point vibrational energy contributions are not included. The heats of formation and reduction energy are summarized in Table IV along with the experimental results at room temperature (298 K).

Table III shows satisfactory agreement between the PAW and L/APW+LO methods. The poorer performance of LDA with respected to PBE is as expected.[57,58] Table III also shows that hybrid PBE0 and HSE functionals significantly diminish the characteristic overestimation of the O_2 atomization energy by the LDA and GGA functionals.[32,39,65,66] However, for bulk Ce, hybrid functionals underestimate the atomization energy with respect to experiment and perform much worse than PBE. Similar problems have been recently reported for the atomization energy of d metals. It has been argued that these discrepancies are related to the overestimation of the exchange splitting in d atoms, with a simultaneous increase of the spin-polarization energy.[33] Thus, the spin-polarized free atom is overstabilized compared to an artificial non-spin-polarized one. Note that errors in the atomic Ce energies will not affect the formation energies reported below. We furthermore note that the HSE and PBE0 functionals

TABLE IV. Reaction energy of $2CeO_2 \rightarrow Ce_2O_3 + (1/2)O_2$ and heat of formation of cerium oxides (in eV).

Method	XC	$\Delta H^{CeO_2 \rightarrow Ce_2O_3}$	$\Delta H_f^{CeO_2}$	$\Delta H_f^{Ce_2O_3}$
PAW[a]	PBE0	3.14	−11.15	−19.18
PAW[a]	HSE	3.16	−11.00	−18.85
PAW[a]	LDA	4.92	−11.49	−18.07
PAW[a]	PBE	4.18	−10.24	−16.30
L/APW+LO[a]	PBE	4.24	−10.35	−16.47
PAW[a]	LDA+U	3.04		
PAW[a]	PBE+U	2.29		
USPP[b]	LDA+U	2.40		
USPP[b]	PBE+U	1.74		
USPP[c]	LDA+U	5.94		
USPP[c]	PBE+U	4.72		
Expt.[d] (298 K)		3.57	−10.62	−17.70
Expt.[e] (298 K)		4.03	−11.30	−18.58

[a]Present work.
[b]Reference 13; using atomiclike functions.
[c]Reference 13; using Wannier-Boys functions.
[d]Reference 5.
[e]Reference 69.

tend to overestimate the spin-polarization energy of magnetic γ-Ce, making it too stable compared to α-Ce, whereas semilocal functionals predict γ-Ce to be too unstable compared to α-Ce. Thus the face transition from α- to γ-Ce is not satisfactorily described by any of the (mean-field) approaches used in the present work.

The results for the heats of formation and reaction energy are summarized in Table IV. A major problem is that the heats of formation are very difficult to measure experimentally, which is related to difficulties in preparing defect-free ceria with a well-defined oxidation state. The most recent experimental values are found in the last row, and they differ from all previous values by up to 1 eV. This uncertainty makes it difficult to put any firm statement on the reliability of the PBE and hybrid functionals for the relative energetics of cerium oxides.

Tentatively, it is, however, clear that the PBE functional underestimates the formation energies and overestimates the reduction energy $\Delta H^{CeO_2 \rightarrow Ce_2O_3}$ albeit only slightly. In all likelihood, the good agreement for $\Delta H^{CeO_2 \rightarrow Ce_2O_3}$ is related to a fortuitous cancellation of errors. A recent investigation of a large number of oxidation reactions for $3d$ metals and simple metals $\left(MO_x + \frac{y-x}{2}O_2 \rightarrow MO_y\right)$ has found that the GGA *underestimates* the reaction energies of oxidation systematically by roughly 1.36 eV/O_2.[70] One can correct for this error, by shifting the O_2 reference energy by 0.68 eV per 1/2 O_2, i.e., by making O_2 less favorable. Applying such a correction brings the absolute formation energies [11.60 eV (CeO_2), 18.34 eV(Ce_2O_3)] indeed into closer agreement with recent experiments, but it also increases the reaction energy $\Delta H^{CeO_2 \rightarrow Ce_2O_3}$ to an unrealistically large value of 4.86 eV. Although such considerations are necessarily rather speculative, they demonstrate that the agreement on the PBE level is fortuitous and not related to a proper description of the underlying bonding properties of CeO_2 and Ce_2O_3.

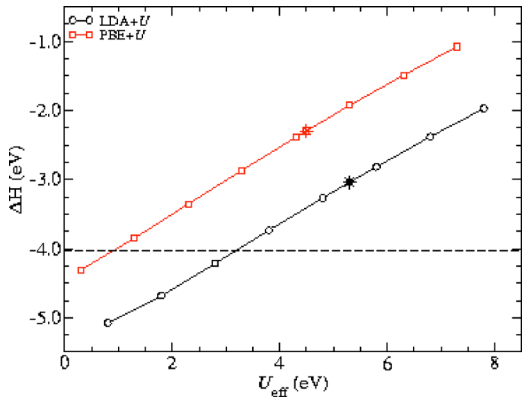

FIG. 5. (Color online) Reaction energy of reduction $2CeO_2 \rightarrow Ce_2O_3 + (1/2)O_2$ as a function of U_{eff}. Energies are determined at the optimized geometries. The stars indicated the results obtained with the calculated U_{eff}. The horizontal dashed line corresponds to the most recent experimental result in Ref. 69.

Using the latest experimental values as a point of reference, the hybrid functionals seem to perform better for the absolute formation energies, but the reduction energy of CeO_2 into Ce_2O_3 is underestimated and predicted to be only 3.14 eV (PBE0) and 3.16 eV (HSE). We have recently calculated the heat of formation of a large number of oxides,[33,71] finding that hybrid functionals consistently underestimate the ΔH_f values, as the PBE functional does; but for the hybrid functionals the error amounts only to roughly 0.3 eV per 1/2 O_2. Correcting for this systematic error yields a reaction energy of about 3.45 eV in reasonable agreement with the experimental estimates, but admittedly such a correction worsens the absolute formation energies slightly. It is fairly obvious that none of the present functionals is able to give a consistent and completely satisfactory picture of the relative formation energies of ceria.

Turning now to the DFT+U approach, we find that LDA+U and PBE+U underestimate the reduction energy $\Delta H^{CeO_2 \rightarrow Ce_2O_3}$ (see Table IV). In the latter case the deviations are fairly large (about 1.3–1.7 eV with respect to the most recent experimental data[69]), whereas the LDA+U method performs better with an underestimation similar to that of the hybrid functionals (0.5–1.0 eV). We reemphasize here that the DFT+U results depend not only strongly on the chosen values of U_{eff} and on the choice of the underlying functional, but also on the nature of the projection orbitals. From the calculated reduction energies as a function of U_{eff} (see Fig. 5), we conclude that the magnitude of $\Delta H^{CeO_2 \rightarrow Ce_2O_3}$ linearly increases with decreasing U_{eff} values, which is in agreement with previously reported DFT+U studies by Fabris *et al.*[13] It is discouraging that the U_{eff} value (~3.25 eV) that corrects the LDA+U reduction energy would yield, for example, a worse (smaller) $E_{g\text{-}f}$ Ce_2O_3 gap and smaller Ce_2O_3 equilibrium volume (see Fig. 2). For the PBE+U case, the situation is similar.

Fabris *et al.*[13] have shown that the linear dependence on the value of U_{eff} can be removed by applying the U term to localized Wannier-Boys functions. Their DFT+U reduction

energies (for the same values of U_{eff} as in this work) with both types of orbitals are reproduced in Table IV. Those calculated with the atomiclike functions are in reasonable agreement with our values; discrepancies are possibly related to the use of ultrasoft pseudopotentials compared to the PAW potentials. The deviations of values obtained with the Wannier-Boys orbitals are considerably large, for the LDA+U in particular. Reportedly the values obtained with the Wannier-Boys orbitals do not depend on U_{eff}.

IV. DISCUSSION

We have reported hybrid DFT Hartree-Fock calculations on CeO_2 and Ce_2O_3 bulk phases with periodic boundary conditions and a plane-wave basis set, and we have compared the results with the standard LDA and PBE cases, as well as the DFT+U approach. The hybrid functionals yield equilibrium volumes in quantitative agreement with experiment, and thus represent a pronounced improvement over the LDA and PBE functionals. For the structural properties, this concerns particularly Ce_2O_3 for which the volume increases from the PBE to the hybrid functionals, opposite to the usual volume decrease from semilocal to hybrid functionals.[28,33] This unusual behavior is related to the localization of a single Ce 4f electron in Ce_2O_3 for hybrid functionals, overcoming the failure of semilocal density functionals that incorrectly describe the 4f electron as delocalized in Ce_2O_3. Therefore, the increase in volume is closely linked to the proper description of the electronic structure.

In general, the HSE functional gives the most balanced description of the electronic properties, with fundamental band gaps and the position of the 4f states being close to experimental values. The local and semilocal functionals fail to yield a sizable band gap between the occupied 4f state and the conduction band in Ce_2O_3. Anyway, a comparison between one-electron energies and the measured quasiparticle spectra must be done with some caution, since (generalized) Kohn-Sham one-electron energies are not related to quasiparticle energies.

For the prediction of thermochemical properties, the hybrid functionals do not appear to provide a clear-cut improvement over the standard PBE functional, although comparison with experiments is rather difficult, since the experimental formation energies are not known very accurately. Most notably, the hybrid functionals underestimate the reduction energy $\Delta H\left(2CeO_2 \rightarrow Ce_2O_3 + \frac{1}{2}O_2\right)$ by roughly 0.9 eV. On the other hand, the formation energy of CeO_2 is predicted very accurately, and that of Ce_2O_3 is overestimated only slightly by 2%, whereas the PBE functional leads to an underestimation by roughly 9% and 12%, respectively. It seems that this is mostly related to a different description of the binding in the O_2 molecule for the hybrid and PBE functionals (cf. Table III). We have furthermore argued that the good agreement of the reduction energy for PBE (4.28 eV) with experiment (4.03 eV) is due to a fortunate error cancellation, and not in line with other simple and transition metal oxides.[70]

Comparison of the PBE0 and HSE, local, and semilocal functionals with the DFT+U results shows that DFT+U gives rather controversial results. Our calculations indicate that LDA+U and PBE+U yield a better account than LDA or PBE for most properties. However, as always, the results depend on the U parameter. The equilibrium lattice constants, the position of the (occupied or unoccupied) 4f states in the band gap, and the reduction energy vary linearly with the effective Hubbard U values. Certainly the DFT+U method does not possess any predictive capabilities, and worse, in the present case, there is no unique U that gives a reasonable account of structural parameters, the relative energies of different oxides, and spectroscopic properties. If one is forced to make a choice, then our calculations suggest that for PBE a very small value of $U_{\text{eff}} \approx 2.0$ eV would give the best overall description for the energetics, lattice constants, and magnetic ordering in Ce_2O_3, instead of the calculated value of 4.50 eV.[13] For LDA, the U_{eff} should be chosen around 3.0–4.0 eV.

We finally note that a recent publication by Hay *et al.*[72] gives very similar results for the structural and electronic properties of CeO_2 and Ce_2O_3 using the LDA, PBE, and HSE functionals. These calculations were carried out using periodic boundary conditions and Gaussian-type orbitals, but did not discuss the thermodynamic properties. Hay *et al.* find a 0.2% underestimated CeO_2 equilibrium volume for the HSE functional. Their LDA and PBE results show the anticipated underestimation (by 2.8%) and overestimation (by 3.2%) of the equilibrium volume, respectively. In this study we find −0.6% (HSE), −2.2% (LDA), and +3.3% (PBE) deviations. For Ce_2O_3, the agreement is similar, namely, −2.0% (HSE), −8.9% (LDA), and −2.0% (PBE) compared to our −0.7% (HSE), −8.9% (LDA), and −2.7% (PBE) data. We observe that in the study by Hay *et al.* the c/a ratio for Ce_2O_3 was held fixed at the experimental value for the HSE functional. The overestimation of the CeO_2 (O 2p–Ce 5d) band gap by ~1 eV for the HSE functional, has been asserted by both Hay *et al.* and the present work. For Ce_2O_3, the HSE predicted $E_{g\text{-}f}$ (Ce 4f-5d 4f) band gap is by 0.8 (Hay *et al.*) and 0.1 eV (this work) overestimated. We note that the screening parameter ω in the HSE functional used in the work by Hay *et al.* might differ from the one (ω =0.158 a.u.) used in the HSE implementation employed in this work.[40]

V. SUMMARY

In summary, the hybrid HSE functional seems to provide a reasonably balanced description of CeO_2 and Ce_2O_3. Most noticeably, the lattice constants can be predicted with roughly 1% precision, and the localization of a single 4f electron in Ce_2O_3 is well described, with the energy of the 4f states even matching measured spectra. It is, however, also clear that significant shortcomings remain, in particular, in the description of the relative energetics. The quest for improved functionals is still open, although it must be emphasized that the present study focuses on one of the most "difficult" elemental oxides in the periodic table.

ACKNOWLEDGMENTS

This work was supported by the Deutsche Forschungsgemeinschaft (Sonderforschungsbereich 546). DFT+LDA/PBE and DFT+U calculations were carried out on the IBM pSeries 690 system of the Norddeutscher Verbund für Hoch- und Höchstleistungsrechnen (HLRN). We thank B. Kallies for technical support. The hybrid PBE0 and HSE functional calculations were carried out in Austria. Support of the Austrian Fonds zur Förderung der wissenschaftlichen Forschung is gratefully acknowledged.

*Electronic address: juarez_dasilva@nrel.gov

[1] J. Kašpar, P. Fornasiero, and N. Hickey, Catal. Today **77**, 419 (2003).
[2] Q. Fu, H. Saltsburg, and M. Flytzani-Stephanopoulos, Science **301**, 935 (2003).
[3] G. A. Deluga, J. R. Salge, L. D. Schmidt, and X. E. Verykios, Science **303**, 993 (2004).
[4] A. Trovarelli, Catal. Rev. - Sci. Eng. **38**, 439 (1996).
[5] A. Trovarelli, *Catalysis by Ceria and Related Materials*, 1st ed. (World Scientific Publishing Company, Singapore, 2002).
[6] V. I. Anisimov, J. Zaanen, and O. K. Andersen, Phys. Rev. B **44**, 943 (1991).
[7] A. V. Prokofiev, A. I. Shelykh, and B. T. Melekh, J. Alloys Compd. **242**, 41 (1996).
[8] H. Pinto, M. H. Mintz, M. Melamud, and H. Shaked, Phys. Lett. **88A**, 81 (1982).
[9] F. Marabelli and P. Wachter, Phys. Rev. B **36**, 1238 (1987).
[10] N. V. Skorodumova, R. Ahuja, S. I. Simak, I. A. Abrikosov, B. Johansson, and B. I. Lundqvist, Phys. Rev. B **64**, 115108 (2001).
[11] S. Fabris, S. de Gironcoli, S. Baroni, G. Vicario, and G. Balducci, Phys. Rev. B **71**, 041102(R) (2005).
[12] G. Kresse, P. Blaha, J. L. F. Da Silva, and M. V. Ganduglia-Pirovano, Phys. Rev. B **72**, 237101 (2005).
[13] S. Fabris, S. de Gironcoli, S. Baroni, G. Vicario, and G. Balducci, Phys. Rev. B **72**, 237102 (2005).
[14] R. L. Martin and F. Illas, Phys. Rev. Lett. **79**, 1539 (1997).
[15] F. Illas and R. L. Martin, J. Chem. Phys. **108**, 2519 (1998).
[16] A. Svane and O. Gunnarsson, Phys. Rev. Lett. **65**, 1148 (1990).
[17] L. Petit, A. Svane, Z. Szotek, and W. M. Temmerman, Phys. Rev. B **72**, 205118 (2005).
[18] A. D. Becke, J. Chem. Phys. **98**, 5648 (1993).
[19] R. Dovesi, C. Roetti, M. Causà, N. M. Harrison, R. Orlando, and E. Aprà, computer code CRYSTAL 1998 (University of Torino, Torino, 1998).
[20] T. Bredow and A. R. Gerson, Phys. Rev. B **61**, 5194 (2000).
[21] J. Muscat, A. Wander, and N. M. Harrison, Chem. Phys. Lett. **342**, 397 (2001).
[22] K. N. Kudin, G. E. Scuseria, and R. L. Martin, Phys. Rev. Lett. **89**, 266402 (2002).
[23] I. P. R. Moreira, F. Illas, and R. L. Martin, Phys. Rev. B **65**, 155102 (2002).
[24] Y.-F. Zhang, W. Lin, Y. Li, K.-N. Ding, and J.-Q. Li, J. Phys. Chem. B **109**, 19270 (2005).
[25] F. Gygi and A. Baldereschi, Phys. Rev. B **34**, 4405 (1986).
[26] S. Chawla and G. A. Voth, J. Chem. Phys. **108**, 4697 (1998).
[27] J. Heyd, G. E. Scuseria, and M. Ernzerhof, J. Chem. Phys. **118**, 8207 (2003).
[28] J. Heyd and G. E. Scuseria, J. Chem. Phys. **120**, 7274 (2004).
[29] J. P. Perdew, M. Ernzerhof, and S. Burke, J. Chem. Phys. **105**, 9982 (1996).
[30] C. Adamo and V. Barone, J. Chem. Phys. **110**, 6158 (1999).
[31] M. Ernzerhof and G. E. Scuseria, J. Chem. Phys. **110**, 5029 (1999).
[32] J. Paier, R. Hirschl, M. Marsman, and G. Kresse, J. Chem. Phys. **122**, 234102 (2005).
[33] J. Paier, M. Marsman, K. Hummer, G. Kresse, I. C. Gerber, and J. G. Ángyán, J. Chem. Phys. **124**, 154709 (2006).
[34] T. Todorova, A. P. Seitsonen, J. Hutter, I.-F. W. Kuo, and C. J. Mundy, J. Phys. Chem. **110**, 3685 (2006).
[35] P. E. Blöchl, Phys. Rev. B **50**, 17953 (1994).
[36] G. Kresse and D. Joubert, Phys. Rev. B **59**, 1758 (1999).
[37] O. Bengone, M. Alouani, P. Blöchl, and J. Hugel, Phys. Rev. B **62**, 16392 (2000).
[38] G. K. H. Madsen, P. Blaha, K. Schwarz, E. Sjöstedt, and L. Nordström, Phys. Rev. B **64**, 195134 (2001).
[39] J. P. Perdew, K. Burke, and M. Ernzerhof, Phys. Rev. Lett. **77**, 3865 (1996).
[40] J. Heyd, G. E. Scuseria, and M. Ernzerhof, J. Chem. Phys. **124**, 219906 (2006).
[41] J. P. Perdew and Y. Wang, Phys. Rev. B **45**, 13244 (1992).
[42] S. L. Dudarev, G. A. Botton, S. Y. Savrasov, C. J. Humphreys, and A. P. Sutton, Phys. Rev. B **57**, 1505 (1998).
[43] M. Cococcioni and S. de Gironcoli, Phys. Rev. B **71**, 035105 (2005).
[44] G. Kresse and J. Hafner, Phys. Rev. B **48**, 13115 (1993).
[45] G. Kresse and J. Furthmüller, Phys. Rev. B **54**, 11169 (1996).
[46] P. Blaha, K. Schwarz, G. Madsen, D. Kvasnicka, and J. Luitz, computer code WIEN2k (Vienna University of Technology, Vienna, 2001).
[47] K. Schwarz, P. Blaha, and G. K. H. Madsen, Comput. Phys. Commun. **147**, 71 (2002).
[48] D. J. Singh, *Plane Waves, Pseudopotentials and LAPW Method* (Kluwer Academic Publishers, Boston, 1994).
[49] E. Sjöstedt, L. Nordstöm, and D. J. Singh, Solid State Commun. **114**, 15 (2000).
[50] H. J. Monkhorst and J. D. Pack, Phys. Rev. B **13**, 5188 (1976).
[51] S. J. Duclos, Y. K. Vohra, A. L. Ruoff, A. Jayaraman, and G. P. Espinosa, Phys. Rev. B **38**, 7755 (1988).
[52] L. Gerward and J. S. Olsen, Powder Diffr. **8**, 127 (1993).
[53] A. Nakajima, A. Yoshihara, and M. Ishigame, Phys. Rev. B **50**, 13297 (1994).
[54] L. Gerward, J. S. Olsen, L. Petit, G. Vaitheeswaran, V. Kanchana, and A. Svane, J. Alloys Compd. **400**, 56 (2005).
[55] H. Bärnighausen and G. Schiller, J. Less-Common Met. **110**, 385 (1985).
[56] F. D. Murnaghan, Proc. Natl. Acad. Sci. U.S.A. **50**, 697 (1944).
[57] M. Fuchs, J. L. F. Da Silva, C. Stampfl, J. Neugebauer, and M.

Scheffler, Phys. Rev. B **65**, 245212 (2002).
[58] J. L. F. Da Silva, C. Stampfl, and M. Scheffler, Surf. Sci. **600**, 703 (2006).
[59] Z. Yang, T. W. Woo, M. Baudin, and K. Hermansson, J. Chem. Phys. **120**, 7741 (2004).
[60] T. Yamamoto, H. Momida, T. Hamada, T. Uda, and T. Ohno, Thin Solid Films **486**, 136 (2005).
[61] S. Fabris, G. Vicario, G. Balducci, S. de Gironcoli, and S. Baroni, J. Phys. Chem. B **109**, 22860 (2005).
[62] E. Wuilloud, B. Delley, W.-D. Schneider, and Y. Baer, Phys. Rev. Lett. **53**, 202 (1984).
[63] P. Wachter, Physica B **300**, 105 (2001).
[64] J. Donohue, *The Structure of the Elements* (John Wiley & Sons, New York, 1974).
[65] B. Hammer, L. B. Hansen, and J. K. Norskov, Phys. Rev. B **59**, 7413 (1999).
[66] J. Sauer and J. Döbler, Dalton Trans. **19**, 3116 (2004).
[67] C. Kittel, *Introduction to Solid State Physics*, 7th ed. (John Wiley & Sons, New York, 1996).
[68] G. Herzberg, *Molecular Spectra and Molecular Structure I. Spectra of Diatomic Molecules*, 2nd ed. (Robert E. Krieger Publishing Co., Malabar, FL, 1989).
[69] M. Zinkevich, D. Djurovic, and F. Aldinger, Solid State Ionics **177**, 989 (2006).
[70] L. Wang, T. Maxisch, and G. Ceder, Phys. Rev. B **73**, 195107 (2006).
[71] M. Marsmann, J. Paier, C. Franchini, V. Bayer, and G. Kresse (unpublished).
[72] P. J. Hay, R. L. Martin, J. Uddin, and G. E. Scuseria, J. Chem. Phys. **125**, 034712 (2006).